



# Wind Load Characteristics and Load Partition Study of Photovoltaic Array

Bin Zhang<sup>1</sup>, Jiaxing Wang<sup>2\*</sup>, Dongdong Zhang<sup>1</sup>, Mao Yan<sup>2</sup>, Xinling Fan<sup>1</sup>,  
Min Liu<sup>2</sup>, Shidong Nie<sup>2</sup>

<sup>1</sup>PowerChina Guiyang Engineering Corporation Limited, Guiyang. 550081, PR China

<sup>2</sup>School of civil engineering, Chongqing University, Chongqing 400045, PR China

\*Corresponding author E-mail addresses: 2311910398@qq.com

**Abstract.** As global energy demand grows and concern over climate change increases, solar photovoltaic (PV) power generation, as a clean and renewable energy source, has garnered widespread attention and is rapidly developing. Due to the relatively low stiffness of PV modules, their light weight, and large spans, they are typically wind-sensitive structures, making wind loads an important factor. This study, set against the backdrop of the Huarong PV project by China Power Construction Group Guiyang Survey and Design Institute, employs a flexible PV rigid model to conduct wind tunnel pressure tests, examining the wind load characteristics of PV modules under different azimuth angles. The results indicate that the upstream PV panels have a significant shielding effect on the downstream PV panels; areas with higher absolute mean wind pressure exhibit greater fluctuating wind pressure, necessitating consideration of fatigue effects. The findings provide important wind load design references for the application of PV modules in civil engineering projects, contributing to the structural safety and reliability of PV power plants.

**Keywords:** Photovoltaic Array; Wind Tunnel Test; Wind Load Characteristics; Extremes;

## 1 Introduction

Wind tunnel tests can simulate airflow environments under different wind speeds and directions, enabling accurate measurement and assessment of wind load characteristics on photovoltaic components [1][2]. Through wind tunnel tests and Computational Fluid Dynamics (CFD) simulations, it has been found that upstream photovoltaic components cause significant interference effects on downstream ones [3][4]. And for single-row photovoltaic components, lift and drag increase with the tilt angle varying between 10° and 60° [5].

This paper focuses on to investigate the performance characteristics of photovoltaic components under different conditions through wind tunnel tests, delve into the interaction mechanisms between photovoltaic components and wind, and provide a reliable

theoretical basis and technical support for the design and operation of photovoltaic power systems.

## 2 Experiment Introduction and Parameter Definition

The wind tunnel test model is shown in Fig. 1 (a). The photovoltaic array consists of six rows and six columns, with the prototype single-row square array measuring 55m in length, with a spacing of 3.2m between rows, a panel tilt angle of 15°, and a geometric scale ratio of 1/30. In this experiment, a model thickness of 8mm was chosen for ease of pressure tube installation.

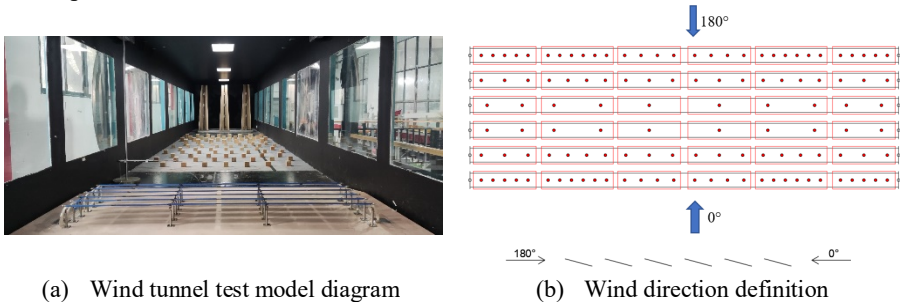


Fig. 1. Wind tunnel test model diagram

A total of 240 measurement points were arranged on the photovoltaic components. The layout of the measurement points is shown in Fig. 1 (b).

To ensure the universality of the experimental results, the pressure time-series data at each measurement point are represented in non-dimensional pressure coefficient form:

$$C_{pi}(t) = \frac{P_i(t) - P_{\infty}}{P_0 - P_{\infty}} \quad (1)$$

$$\bar{C}_{pi} = \frac{1}{N} \sum_{j=1}^N C_{pij} \quad (2)$$

$$C_{pi,rms} = \sqrt{\frac{1}{N-1} \sum_{j=1}^N (C_{pij} - \bar{C}_{pi})^2} \quad (3)$$

$C_{pi}$ ,  $\bar{C}_{pi}$ ,  $rms$  represent the mean and root mean square of the pressure coefficient, while  $N$  is the number of sampling points in the sample.

The wind tunnel test utilized a Class B terrain wind field standard. In the wind tunnel, rough elements and sharp edges were used to simulate wind field information, obtaining experimental wind profiles and turbulence profiles, as shown in Fig. 2.

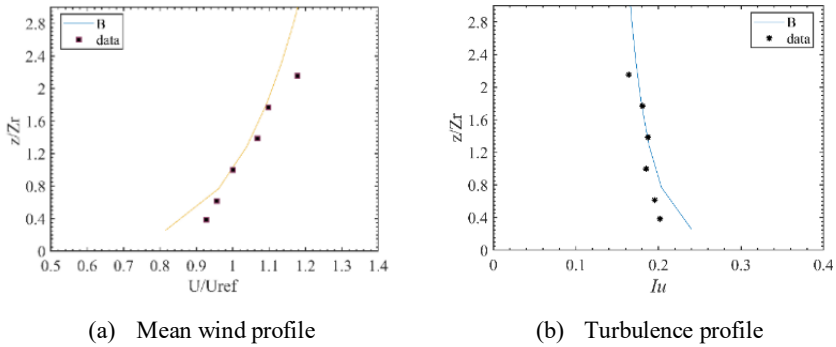


Fig. 2. Wind field simulation results

### 3 Wind Load Characteristics Analysis

#### 3.1 Average Pressure Coefficients

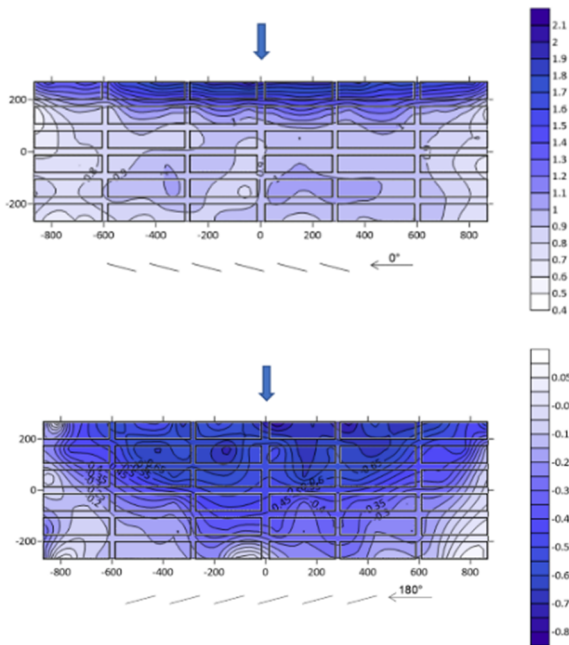


Fig. 3. Net wind pressure Average wind pressure coefficient

When the inflow wind direction is  $0^\circ$ , the wind load on the front row of photovoltaic panels exhibits a significant gradient change with relatively large values, leading to a considerable overturning moment. The wind load on the rear row, due to the shielding

effect of the front row panels, stabilizes and is approximately half of the front row's values. Fig. 3 illustrates that at a  $180^\circ$  wind direction, the entire photovoltaic assembly experiences wind suction and shows a noticeable gradient change. The wind load variation is more uniform with no distinct sudden changes.

### 3.2 Fluctuating Wind Pressure Coefficients

The distribution pattern of fluctuating wind pressure coefficients as shown in Fig. 4 is similar to that of average wind pressure coefficients. Due to the influence of the incoming wind, the fluctuating values of the wind pressure coefficients on the front row of photovoltaic panels are relatively high. The rear photovoltaic panels experience lower fluctuating wind pressure coefficients due to the shielding effect of the front row panels.

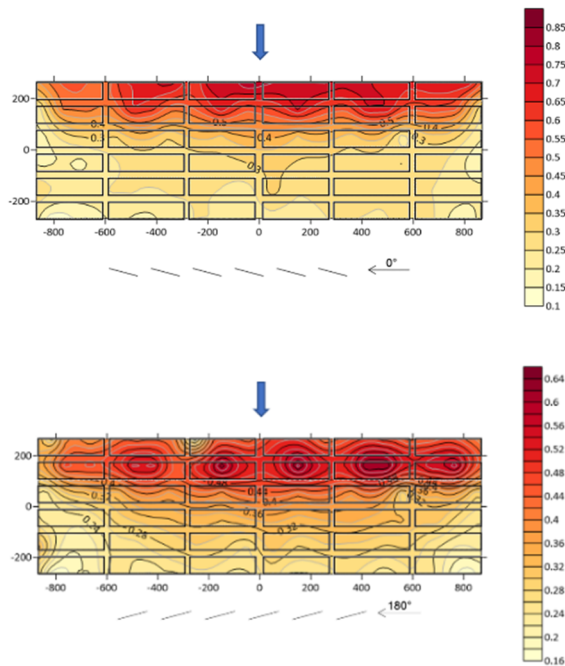


Fig. 4. Net wind pressure fluctuating wind pressure coefficient

### 3.3 Extreme Wind Pressure Coefficients

The extreme calculation method employed in this study is based on the PHPM model proposed by Liu et al. [6], which introduces a new statistical moment definition without feasible area restrictions. The specific calculation results are as follows: Fig. 5 show the contour maps of the net wind pressure extreme wind pressure coefficients at wind directions of  $0^\circ$  and  $180^\circ$ , respectively. Table 1 presents the extreme wind pressure coefficients for each photovoltaic panel. Similar to the distribution patterns of average and fluctuating wind pressure coefficients, the extreme wind pressure coefficients of

the photovoltaic panels on the left and right sides exhibit symmetrical distributions and noticeable gradient changes.

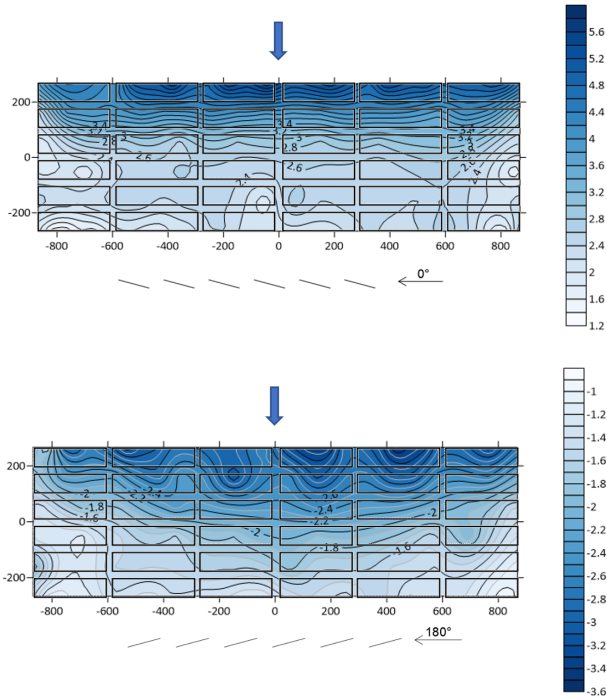


Fig. 5. 180°Net minimum wind pressure coefficient

Table 1. 0°Extreme wind pressure coefficient

	Row1	Row2	Row3	Row4	Row5	Row6
0°	4.90	3.78	2.56	2.29	2.35	2.01
180°	-2.83	-2.37	-1.87	-1.60	-1.46	-1.26

### 4 Conclusion

(1) The upstream photovoltaic panels exhibit a significant shielding effect on the downstream panels. The first and second photovoltaic components have the highest wind pressure coefficients (including average, fluctuating, and extreme wind pressure coefficients), while the size coefficient of the third photovoltaic component is noticeably lower than the first two components. The size coefficient of the rear panels tends to stabilize, indicating the impact of upstream panels on downstream panels.

(2) Under wind directions of 0° and 180°, the distribution patterns of average wind pressure are similar to those of fluctuating wind pressure. Regions with higher absolute values of average wind pressure correspond to larger fluctuating wind pressure values.

This implies that areas with high wind pressure on the photovoltaic panel surface experience more unstable wind loads. When designing photovoltaic support structures, consideration should be given not only to the damage caused by extreme wind loads but also to the impact of fatigue on the photovoltaic components.

(3) Limitations and Future Work: Conduct wind tunnel tests at multiple wind direction angles to investigate the effect of wind direction on the distribution of wind loads; utilize numerical simulation techniques to explore the underlying mechanisms.

## Reference

1. Yang, Q.S., Shan, W.S., Tamura, Y. (2023) Characteristics of fluctuating wind loads on high-rise buildings. *China Civil Engineering Journal.*, 56(05):1-17+88. DOI: 10.15951/j.tmgcx.2023.05.22121220.
2. Wang, J.X., Yang, Q.S., Hui, Y. (2021) Comparisons of design wind pressures on roof-mounted solar arrays between wind tunnel tests and codes and standards. *Advances In Structural Engineering.*, 24(04): 653-666. DOI:10.1177/1369433220965274.
3. Li, J.Q., He, Y.L., Xu, Z.H. (2019) Analysis of wind load shielding effect of array photovoltaic panel. *Shanxi Architecture.*, 45(20):54-56. DOI: 10.13719/j.cnki.cn14-1279/tu.2019.20.028.
4. Ma W.Y, Ma C.C, Wang C.Y, et al. (2021) Wind tunnel experimental study on the wind load interference effect of photovoltaic arrays. *Experimental Fluid Mechanics*, 35(04): 19-25. Doi:10.11729/syltlx20200127.
5. Irtaza, H., Agarwal, A. (2018) CFD Simulation of Turbulent Wind Effect on an Array of Ground-Mounted Solar PV Panels. *Journal of The Institution of Engineers (India): Series A*, 99(2):205-218. <https://doi.org/10.1007/s40030-018-0283-x>.
6. Liu, M., Chen, X.Z., Yang, Q.S. (2017) Estimation of Peak Factor of Non-Gaussian Wind Pressures by Improved Moment-Based Hermite Model. *Journal of Engineering Mechanics*, 143(7). DOI:10.1061/(ASCE)EM.1943-7889.0001233.

**Open Access** This chapter is licensed under the terms of the Creative Commons Attribution-NonCommercial 4.0 International License (<http://creativecommons.org/licenses/by-nc/4.0/>), which permits any noncommercial use, sharing, adaptation, distribution and reproduction in any medium or format, as long as you give appropriate credit to the original author(s) and the source, provide a link to the Creative Commons license and indicate if changes were made.

The images or other third party material in this chapter are included in the chapter's Creative Commons license, unless indicated otherwise in a credit line to the material. If material is not included in the chapter's Creative Commons license and your intended use is not permitted by statutory regulation or exceeds the permitted use, you will need to obtain permission directly from the copyright holder.

